Published by IOP Publishing for Sissa Medialab

Received: *January 21, 2020*
Accepted: *February 26, 2020*
Published: *April 6, 2020*

Plasma Physics by Laser and Applications (PPLA 2019)
Physics Department, University of Pisa, Pisa, Italy
29–31 October, 2019

Geometric and electromagnetic characterization of electron beams produced by nanodiamond photocathodes

L. Velardi,[a,b] **G. Quarta,**[a,b] **L. Calcagnile,**[a,b] **V. Nassisi**[a,b] **and G. Cicala**[c]

[a] *Department of Physics, University of Salento, via per Arnesano, 73100, Lecce, Italy*
[b] *INFN section of Lecce, Lecce, Italy*
[c] *CNR-ISTP, Via Amendola 122/D, 70126 Bari, Italy*

E-mail: luciano.velardi@le.infn.it

Abstract: In this work, the geometric and electromagnetic characteristics of electron beams generated by three photocathodes (PCs), two based on nanodiamond (ND) layers and one based on Cu (generally used as reference) were investigated. Specifically, the active layers of the ND-based PCs consisted of untreated and hydrogenated (H-ND) nanoparticles (250 nm in size) deposited by pulsed spray technique on *p*-doped silicon substrates as uniform coating. Photoemission measurements carried out by a KrF nanosecond excimer laser (λ = 248 nm) in a vacuum chamber at 10^{-6} mbar and the emittance evaluation, performed by the *pepper pot* method, are reported and discussed. For the last, radio-chromic films (HD-810 Gafchromic) were used as sensible screen for electrons. The study of the emittance was performed by varying the laser spot onto the PC surface and the accelerating voltage (5, 10 and 15 kV). From emittance values, the normalized brightness was also estimated for all the cathodes. The obtained results showed quantum efficiency values of the ND-based photocathodes higher than that of the reference Cu one, but, at the same time, higher emittances and therefore worse performancers as the result of the enlarged beam divergence. Despite this, H-ND resulted to be the best PC between those investigated for the highest normalized beam brightness, thanks to its high electron current and low normalized emittance.

Keywords: Photoemission; Photon detectors for UV, visible and IR photons (solid-state)

https://doi.org/10.1088/1748-0221/15/04/C04017

Contents

2020 JINST 15 C04017

1 Introduction

Nowadays, the photocathodes (PCs) represent a fundamental component to produce electron beams for injectors in linear accelerators [1], synchrotrons, free electron lasers [2–4] and so on. Semiconductors [3, 5–9] and metals [3, 10, 11] are the materials employed in the photocathode production which require good quantum efficiency, good lifetime/robustness, fast response time and low emittance. About the PCs based on semiconductors, the active layers are generally made of CsI, Cs_3Sb, Cs_2Te, GaAs, and GaN. In the last two decades, the diamond has been found operating in the ultraviolet range as an important wide-bandgap semiconductor for photocathode. The diamond is well known for its superior chemical-physical properties (high chemical inertness, high mechanical hardness, high radiation hardness, etc) but it is also very interesting for its optoelectronic properties, thanks to the wide gap of 5.47 eV and low electron affinity of 0.35–0.5 eV [12] that becomes negative (NEA, −1.27 eV) when its surface is hydrogenated [13, 14]. A NEA means that the vacuum level shifts beneath of conduction band minimum and therefore the electrons injected in the conduction band are emitted directly into the vacuum, enhancing the photoemission.

The technology of diamond films is today based on chemical vapour deposition (CVD) methods [15–19], which work at high substrate temperatures (> 600°C). In the last years, new techniques have been developed, to overcome the limit of the high deposition temperature and to allow different possibilities in terms of materials used as carbon sources. One of these is the pulsed spray technique [20, 21], a cheap and straightforward method which allows the deposition of layers at low temperature (∼ 150°C), starting from a dispersion of nanodiamond (ND) particles in pure water. Indeed, high efficiency UV photocathodes based on nanodiamond layers [8, 9, 22] have been produced and characterized in the vacuum ultraviolet spectral range (140–210 nm).

The aim of this paper is to study the geometric and electromagnetic properties of electron beams produced by photoemission from ND-based photocathodes (PCs), in order to obtain an electron source with low emittance, high brightness and good output charge. For this reason, two photocathodes, based on untreated and hydrogenated nanodiamond (ND) layers were examined.

These PCs were compared to a Cu one, used as reference. The photoemission measurements were carried out in vacuum by a KrF excimer laser, whereas the emittance evaluation was performed by the *pepper pot* method [23]. The brightness of the PCs was also estimated by emittance values.

2 Materials and methods

2.1 Photocathodes

Three photocathodes were characterized: two based on ND layers and one based on a pure (99.9%) Cu sample, 500 µm thick, provided by Goodfellow. The ND-based PCs were fabricated starting from as-received (untreated ND_{ar}) and hydrogenated (treated H-ND) nanodiamond powders with an average grain size of 250 nm, marketed by Diamonds & Tools srl. The hydrogenation of the ND particles was performed in H_2 microwave plasma [8, 9], in an *ASTeX*-type reactor. All the powders were then dispersed in deionized water, sonicated for 30 min by a Bandelin Sonoplus HD2070 system and then deposited by pulsed spray technique [8, 9] on *p*-doped silicon substrates, 12×12 mm^2. The number of the pulses was set to 400 for both the ND photocathodes, obtaining a thickness around 10 µm (measured by a profilometer). During the spray process, the temperature of the substrate was maintained constant at 150°C (to speed up the evaporation of the solvent), a value much lower than those typically used in CVD techniques (> 600°C).

2.2 Photoemission measurement

The photoemission measurements were carried out in reflective mode. Figure 1a shows a sketch of the experimental apparatus used which consists of a KrF excimer laser (λ = 248 nm and τ = 23 ns at full-width at half-maximum, FWHM), a photodiode (*Ph*), a beam-splitter (*B*), a mirror (*M*), a thin lens (*L*) and a vacuum stainless-steel chamber equipped with a quartz window (*W*), a vacuum system, a holder for photocathode (*PC*) and some capacitors (*C*). The anode was indicated with (*A*) and the anode voltage with V_a. The anode-cathode distance was set at 3 mm and the accelerating voltage was varied from 0.15 to 15 kV. Values higher than 15 kV caused the electrical breakdown in the accelerating gap. The beam splitter was utilized to divide the laser beam in two: the first beam was focused by the lens (*L*, 100 cm focal length) producing a spot dimension of 25 mm^2 on the photocathode surface and the fluence resulted to be 0.01 J/cm^2; the second one was sent to a fast photodiode (type Hamamatsu R1328U-02) in order to measure the evolution time of the laser pulse, and to trigger the oscilloscope. Each photocathode was fixed on the holder, i.e. an electric stem connected to the chamber by an insulating flange. Four high voltage capacitors (*C*) of 350 pF/40 kV, connected between *A* and chamber walls (ground), were used to stabilize V_a during the emission and to allow measurements of long pulses. The cathode holder and the chamber walls were considered as a transmission line, with its characteristic impedance of about 50 Ω. Therefore, to avoid signal reflections and to record real current pulses, PC was connected to the ground by a shunt of 50 Ω [24]. It was composed by 9 parallel resistors of approximately 500 Ω and a resistor of 450 Ω connected in series to a 50 Ω coaxial cable (R_{cable}), as shown in the scheme of figure 1a. The signal was transmitted to the oscilloscope through the R_{cable}. The photoelectric charge was measured as a function of the voltage applied between *A* and *PC*. The anode was represented by a stainless-steel grid with 4 meshes per mm^2. The laser intensity transmitting through the anode grid resulted to be of 60%.

2020 JINST 15 C04017

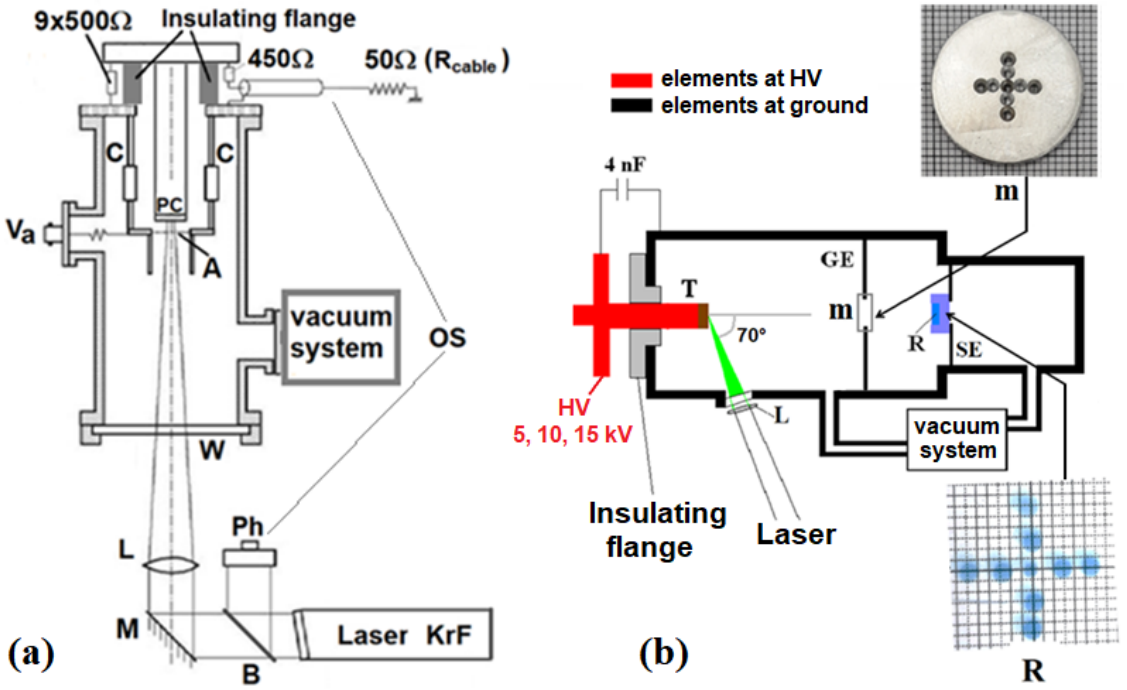

Figure 1. (a) Scheme of the experimental apparatus used to measure the photoemission: KrF excimer laser; Ph: photodiode, B: beam-splitter, M: mirror, L: lens, W: quartz window, C: capacitors, V_a: anode voltage connector, A: anode, PC: photocathode, OS: oscilloscope. (b) Scheme of the experimental apparatus devoted for the emittance evaluation: GE: ground electrode, L: lens, T: target support, m: mask, R: radiochromic film, SE: secondary electrode.

2.3 Emittance measurement

The emittance evaluation was carried out by the *pepper pot* method [23]. Figure 1b shows a sketch of the experimental apparatus used for this measurement. The laser was the same KrF excimer used for photoemission measurements, but the vacuum chamber was different. The energy fluence was maintained constant to 0.01 J/cm^2 in all the experiments. The laser beam was focused by a thin lens (*L*) of 15 cm focal length onto the *PC* surface, forming an angle of 70° with the perpendicular straight line to the target support as shown in figure 1b. This configuration permitted to use the *pepper pot* method so that the laser beam did not interact with the emitted electrons. Three different spot areas (2, 5 and 25 mm^2) were set for the experiment. The accelerating system consisted of three parts: a positive high voltage (*HV*) applied to the target support (*T*), a pierced ground electrode (*GE*) placed at 10 cm distance from T and a secondary ground electrode (*SE*) placed at 5 cm far from *GE*. Four capacitors (each one of 1 nF), between T and ground, were used to stabilize the accelerating voltage during the electron extraction.

The accelerating voltages utilized in the emittance measurement were 5, 10 and 15 kV and the corresponding electric field of the accelerating gap resulted of 0.05, 0.10 and 0.15 MV/m, respectively. The mask (*m*) was made of aluminium and was fixed on the GE. The mask had nine holes of 1 mm in diameter forming a cross and the centre of each hole was at 1.5 mm from each other (see the photo of the mask in figure 1b). Radiochromic films (*R*) Gafchromic HD-810, placed

2020 JINST 15 C04017

on SE, were used as photo-sensible screen.

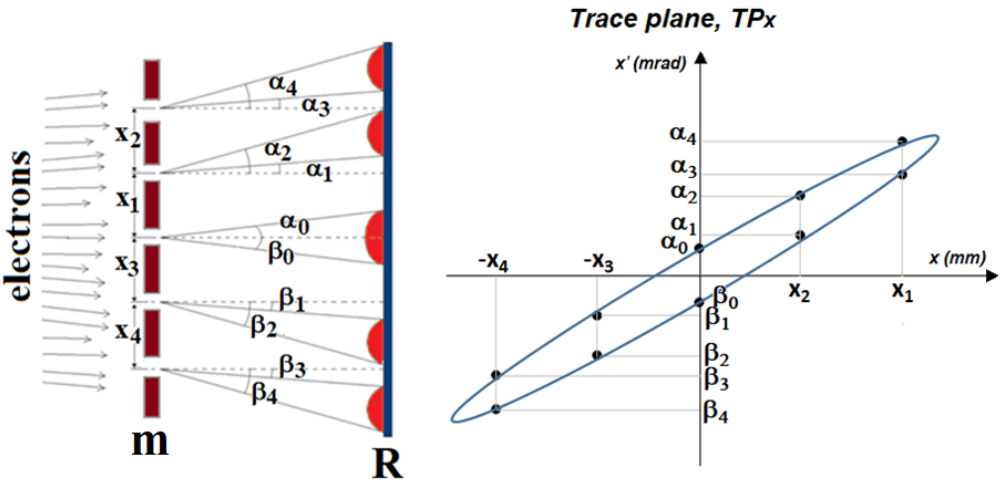

Figure 2. Sketch of the technique used to measure and calculate the emittance diagram by *pepper pot* method [23].

The x-plane emittance ε_x for a z-axis beam propagation is $1/\pi$ times the area A_x in the xx' trace plane (TP_x) occupied by the points representing the beam particles at a given value of z is $\varepsilon_x = A_x/\pi$. The normalized emittance is defined as $\varepsilon_{xn} = \beta\gamma\varepsilon_x$ where $\beta = v/c$ (ratio between the relative v and light c velocities) and $\gamma = 1/(1-\beta^2)^{1/2}$ is the Lorentz factor. Such value does not depend on the acceleration of the particles, if the saturation regime is respected. Figure 2 represents a scheme helpful to understand the method used to draw and calculate the emittance diagram in the trace plane.

3 Results and discussion

Figure 3 shows the photo-charge extracted from Cu, ND_{ar} and H-ND -based photocathodes obtained at the laser fluence of 0.01 J/cm^2, as a function of the accelerating voltage and the electric field (calculated between anode and cathode) reported in lower and upper x-axes, respectively. The logarithmic scales of the x and y -axes better highlight the variation range of two and three orders of magnitude of the voltage and of the extracted charge, respectively. The red straight line (circles) represents the charge calculated from the Child Langmuir (C-L) equation [25].

Figure 4a shows, as example, the emittance diagrams in the TP_x plane for the three photocathodes measured by the *pepper pot* method at the smallest spot of 2 mm^2 and at the lowest accelerating voltage of 5 kV. For the emittance assessment, the ellipse areas, i.e. the values of A_x in the TP_x plane were computed. Figure 4b shows the trend of A_x (expressed in mm mrad) as a function of the accelerating voltage, for the three photocathodes, calculated at the smallest spot of 2 mm^2. It should be noted that the enhancement of the electron charge consequently enlarges the beam divergence for the repulsion among the electrons. This was the reason of the observed increase of emittance by increasing the accelerating voltage (the enhancement of the photocharge is well visible in the investigated range of 0.05–0.15 MV/m, see figure 3) and of the better emittance exhibited by Cu-

2020 JINST 15 C04017

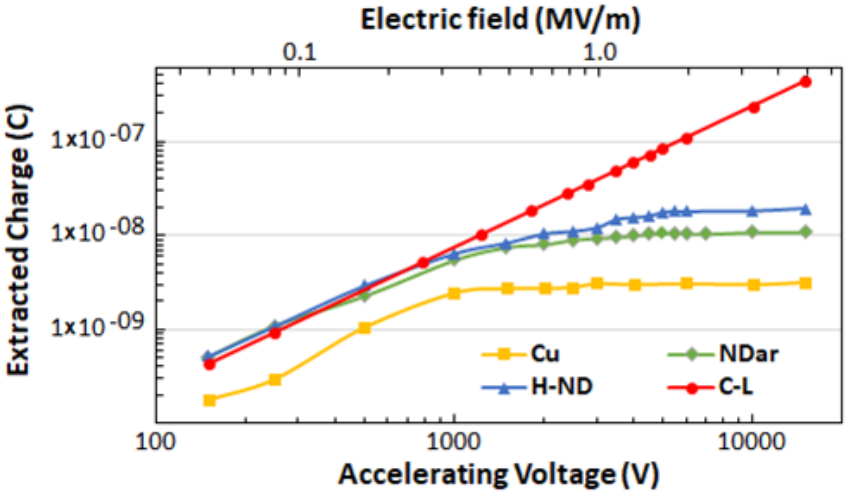

Figure 3. Photo-charge extracted from Cu, ND_{ar} and H-ND -based photocathodes as a function of the accelerating voltage and the electric field at the laser fluence of 0.01 J/cm^2. The red line is the charge calculated from the Child-Langmuir (C-L) equation [25].

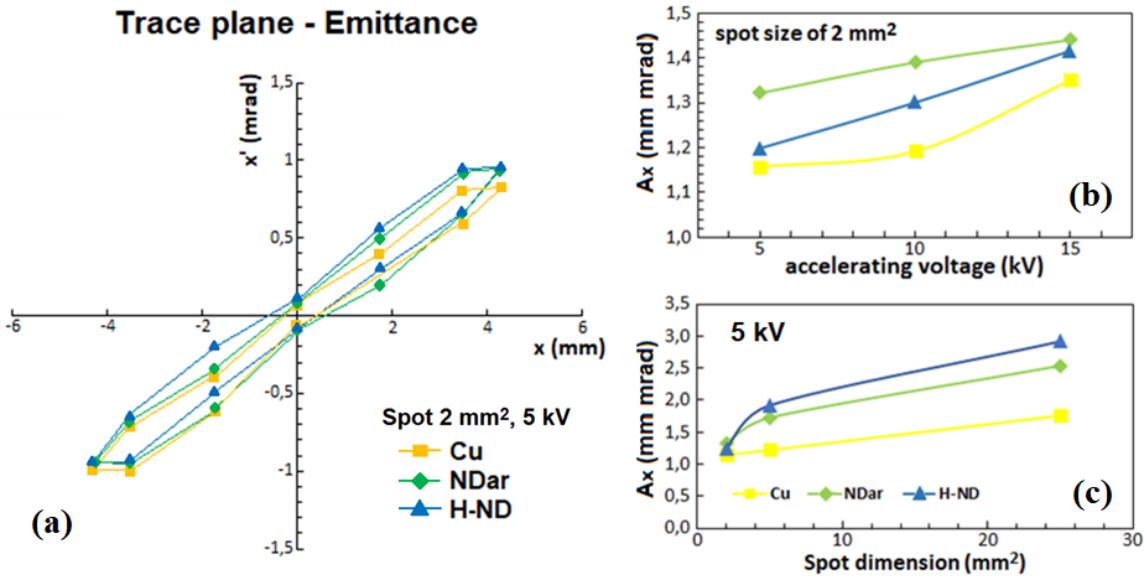

Figure 4. (a) Emittance diagrams in the *xx'* trace plane for the three photocathodes (laser spot: 2 mm^2, accelerating voltage: 5 kV). A_x values for the three photocathodes as a function of the (b) accelerating voltage, calculated at the smallest spot of 2 mm2 and (c) the laser spot area evaluated at the lowest accelerating voltage of 5 kV.

based photocathode (lowest photocurrent than ND-based ones, see figure 3). On the contrary, the emittance of H-ND (although showed the highest photocurrent) resulted lower than that of ND_{ar} and it was attributed to its NEA surface. It is well known, indeed, that NEA photocathodes are bright electron sources with low emittance. Figure 4c shows the trend of A_x fixing the accelerating voltage at 5 kV and varying the laser spot area. The emittance enhancement was observed by increasing

2020 JINST 15 C04017

the spot dimension and was more pronounced in ND-based photocathodes, because of their higher extracted photocharge. The normalized emittance ε_{xn} for all the photocathode resulted of about 0.2 π mm mrad at 5 kV (0.16 for Cu, 0.19 for ND_{ar} and 0.17 for H-ND) and around 0.25 and 0.35 π mm mrad at 10 and 15 kV, respectively. These values were calculated at the smallest spot size of 2 mm^2. From figure 3 it was also possible to calculate the value of the current relatively to the 2 mm^2 spot. Considering the pulse laser duration 23 ns, the extract current ($I = \Delta q/\Delta t$) at 15 kV of accelerating voltage resulted of 1.83×10^{-8} C/23 ns, 1.10×10^{-8} C/23 ns and 3.2×10^{-9} C/23 ns, for the H-ND, ND_{ar} and Cu cathodes, respectively. Assuming the y-direction emittance ε_y equal to ε_x, the normalized beam brightness is definite as $B = I/\varepsilon_{xn}^2$ where I is the total electron current.

Table 1 reports the values of quantum efficiency (QE), normalized emittance, extracted charge, current intensity and brightness of the three PCs, obtained under the above-described experimental conditions. The reported QE values were evaluated at the maximum accelerating voltage of 15 kV, in which the extracted current achieved the saturation. As expected, at the laser wavelength of 248 nm, the ND-based photocathodes resulted more efficient than the Cu one. This is due to the well known optical properties of the diamond in the UV region [26–28] and to the graphite component of the ND powder that plays a fundamental role in the enhancement of the photoemission [8, 9, 29, 30]. The highest QE found for the hydrogenated photocathode (H-ND) was due to the NEA character of its hydrogenated surface. The H-ND photocathode showed also the highest normalized beam brightness thanks to its high electron current and low normalized emittance.

Table 1. Values of quantum efficiency (QE), normalized emittance, extracted charge, current intensity and brightness of the three investigated PCs.

Photocathodes	Cu	ND_{ar}	H-ND
QE (electrons/photons)	0.4×10^{-5}	1.7×10^{-5}	4.0×10^{-5}
normalized emittance ε_{xn}at 5 kV [π mm mrad]	0.16	0.19	0.17
normalized emittance ε_{xn}at 10 kV [π mm mrad]	0.24	0.28	0.26
normalized emittance ε_{xn}at 15 kV [π mm mrad]	0.34	0.36	0.35
Extract charge at 15 kV [C]	0.32×10^{-8}	1.10×10^{-8}	1.83×10^{-8}
Current intensity at 15 kV [A]	0.14	0.48	0.80
Brightness at 15 kV [A/(π m rad)^2]	4.1×10^{11}	1.3×10^{12}	2.3×10^{12}

4 Conclusions

In conclusion, this study evidenced and highlighted that the photoemission properties of the two ND based PCs were more performant than those of Cu based one. The best was the H-ND based PC for the NEA character of its hydrogenated surface that favours the electron emission.

As for the emittance measurements the Cu photocathode exhibited the lowest value that was due to its low extracted charge, less affected by divergence. Despite this, the experiment showed that H-ND is the best PC for the highest normalized beam brightness, thanks to its high electron current and low normalized emittance (little bit higher than Cu). The emittance measurements revealed also that an increase of the accelerating voltage caused an enlargement of the beam (for

2020 JINST 15 C04017

the enhancement of the extracted charge) and therefore, a worsening of the geometric quality of the electron beam. To overcome this issue, it could be necessary to work in saturation regime (electric fields > 2 MV/m under the reported experimental conditions), which involved the use of higher voltage values.

References

[1] A. Todd, *State-of-the-art electron guns and injector designs for energy recovery linacs (ERL)*, *Nucl. Instrum. Meth.* **A 557** (2006) 36.

[2] L. Giannessi et al., *Seeding experiments at SPARC*, *Nucl. Instrum. Meth.* **A 593** (2008) 132.

[3] S.H. Kong et al., *Photocathodes for free electron lasers*, *Nucl. Instrum. Meth.* **A 358** (1995) 272.

[4] C. Bostedt et al., *Experiments at FLASH*, *Nucl. Instrum. Meth.* **A 601** (2009) 108.

[5] O. Siegmund et al., *Development of GaN photocathodes for UV detectors*, *Nucl. Instrum. Meth.* **A 567** (2006) 89.

[6] C. Feng et al., *Optimized chemical cleaning procedure for enhancing photoemission from GaAs photocathode*, *Mater. Sci. Semicond. Process.* **91** (2019) 41.

[7] C. Hernandez-Garcia et al., *Charge production studies from Cs_2 Te photocathodes in a normal conducting RF gun*, *Nucl. Instrum. Meth.* **A 871** (2017) 97.

[8] L. Velardi et al., *Highly efficient and stable ultraviolet photocathode based on nanodiamond particles*, *Appl. Phys. Lett.* **108** (2016) 083503.

[9] L. Velardi et al., *UV photocathodes based on nanodiamond particles: Effect of carbon hybridization on the efficiency*, *Diam. Relat. Mater.* **76** (2017) 1.

[10] J. Scifo et al., *Nano-machining, surface analysis and emittance measurements of a copper photocathode at SPARC_LAB*, *Nucl. Instrum. Meth.* **A 909** (2018) 233.

[11] L. Cultrera et al., *Pulsed laser deposition of Mg thin films on Cu substrates for photocathode applications*, *Appl. Surf. Sci.* **248** (2005) 397.

[12] J. Robertson and M.J. Rutter, *Band diagram of diamond and diamond-like carbon surfaces*, *Diam. Relat. Mater.* **7** (1998) 620.

[13] F.J. Himpsel et al., *Quantum photoyield of diamond(111) — A stable negative-affinity emitter*, *Phys. Rev.* **B 20** (1979) 624.

[14] J.B. Cui, J. Ristein and L. Ley, *Low-threshold electron emission from diamond*, *Phys. Rev.* **B 60** (1999) 16135.

[15] J.J. Gracio et al., *Diamond growth by chemical vapour deposition*, *J. Phys.* **D 43** (2010) 374017.

[16] K. Paprocki et al., *The comparative studies of HF CVD diamond films by Raman and XPS spectroscopies*, *Opt. Mater.* **95** (2019) 109251.

[17] G. Cicala et al., *Study of polycrystalline diamond deposition by continuous and pulsed discharges*, *Surf. Coat. Technol.* **204** (2010) 1884.

[18] G. Cicala et al., *Toward smooth MWPECVD diamond films: Exploring the limits of the hydrogen percentage in Ar/H_2/CH_4 gas mixture*, *Surf. Coat. Technol.* **211** (2012) 152.

[19] M. Breiter et al., *Diamond synthesis with a DC plasma jet: control of the substrate temperature*, *Diam. Relat. Mater.* **9** (2000) 333.

2020 JINST 15 C04017

[20] G. Cicala et al., *Self-Assembled Pillar-like Structures in Nanodiamond Layers by Pulsed Spray Technique*, *ACS Appl. Mater. Interfaces* **6** (2014) 21101.

[21] G. Cicala et al., *Enhancement of surface electrical current on silicon via nanodiamond particles deposited by pulsed spray technique*, *Phys. Status Solidi* **A 212** (2015) 2862.

[22] A. Valentini, D. Melisi, G. De Pascali, G. Cicala, L. Velardi and A. Massaro, *High-efficiency nanodiamond-based ultraviolet photocathodes*, International Patent n. WO/2017/051318 (2017).

[23] J.G. Wang et al., *Beam emittance measurement by the pepper-pot method*, *Nucl. Instrum. Meth.* **A 307** (1991) 190.

[24] L. Velardi et al., *Electron beams produced by innovative photocathodes based on nanodiamond layers*, *Phys. Rev. Accel. Beams* **22** (2019) 093402.

[25] C.D. Child, *Discharge From Hot CaO*, *Phys. Rev. (Series I)* **32** (1911) 492.

[26] D. Vouagner et al., *Photoemission characteristics of diamond films*, *Appl. Surf. Sci.* **168** (2000) 79.

[27] A.S. Tremsin and O.H.W. Siegmund, *UV photoemission efficiency of polycrystalline CVD diamond films*, *Diam. Relat. Mater.* **14** (2005) 48.

[28] G. Cicala et al., *Photo- and thermionic emission of MWPECVD nanocrystalline diamond films*, *Appl. Surf. Sci.* **320** (2014) 798.

[29] W. Zhu et al., *Low-Field Electron Emission from Undoped Nanostructured Diamond*, *Science* **282** (1998) 1471.

[30] J.B. Cui et al., *Role of hydrogen on field emission from chemical vapor deposited diamond and nanocrystalline diamond powder*, *J. Appl. Phys.* **88** (2000) 3667.

2020 JINST 15 C04017